Biomedical Signal Processing and Control 32 (2017) 57–68

Contents lists available at ScienceDirect

Biomedical Signal Processing and Control

journal homepage: www.elsevier.com/locate/bspc

Stationary versus bifurcation regime for standing wave central pattern generator☆

R. Martin del Campo, E. Jonckheere*

Electrical Engineering Dept., University of Southern California, Los Angeles, CA 90089-2563, United States

ARTICLE INFO

Article history:
Received 2 July 2015
Received in revised form 27 May 2016
Accepted 19 August 2016

Keywords:
Central pattern generator
Surface electromyography
Bifurcation
Coherence
Wavelets
Bootstrapping

ABSTRACT

The purpose of this research is to show that the correlation analysis on surface electromyographic (sEMG) signals that originally confirmed existence of a standing wave central pattern generator (CPG) along the spine are reproducible despite evolution of the entrainment technique, different hardware and data collection protocol. Moreover, as major novelty of the present research, it is shown that this CPG can undergo "bifurcations," here revealed by signal processing extrapolated towards the period-halving dynamical interpretation. The visually intuitive manifestation of the bifurcation is statistically confirmed—using bootstrap analysis—by a shift in the cross power spectral densities, consistently with the standing wave occurring on different subbands of the Daubechies DB3 wavelet decomposition of the sEMG signals.

1. Introduction

1.1. Background

The so-called *spinal wave* [1] is a visually obvious phenomenon during which the spine goes through a rhythmic [2] oscillation elicited by light finger pressure at some sensitized areas of the spine, typically, the neck and the sacrum. As argued in our original work [1], Alf Breig's dural-vertebral attachments [3] close sensory-motor loops in both the neck and the sacrum, creating localized oscillations, which soon propagate along the spine to settle in a standing wave pattern. The crucial features that the movement is rhythmic, that after some initial stimulus it becomes self-sustained and hence has no sensory input, already point to a central pattern generator (CPG), a concept that is still an active area of research [4]. Moreover, as reported in the earlier paper [1], a quadriplegic subject with a C2-C3 injury was able to experience some spinal wave pattern, which indicates that the CPG circuitry is embedded in the spine. Circuit diagrams of the CPG were proposed in [1]. It therefore appears that this movement is, next to gait, another human CPG.

Objectively, the *standing wave* aspect of the CPG was confirmed by observing that the correlation pattern among the cervical, thoracic, lumbar and sacral surface electromyographic (sEMG) signals is consistent with that of a standing wave. This correlation pattern appears most clearly on the D_8 subband of the Daubechies DB3 wavelet decomposition. The choice of the DB3 wavelet decomposition is justified because its mother function mimics the single motor unit action potential, and the D_8 subband appeared the most relevant as the electro-physiological phenomena appear on that subband, while the D_1, D_2, ... subbands are composed mostly of high frequency noise [5].

A standing wave oscillation is certainly a manifestation of *coherence* in the neuro-skeletal system. Since the spinal standing wave has its coherence extending from the neck to the sacrum, it is fair to say that this is a phenomenon of *coherence at a distance* [6]. Coherence at a distance between EEG and/or (s)EMG signals is considered to be a sign of the nervous system able to coordinate activities of many muscles towards a specific motion [6]. The additional evidence that we presented in support of this paradigm is the deterioration of coherence in a quadriplegic subject compared with a control subject [1].

1.2. Contribution

The purpose of this paper is threefold. First ("Case Study I"), we show that the early results [1] upon which the CPG hypothesis rests are reproducible. Second ("Case Study II"), we show that the spinal wave CPG, in addition to the classical attributes associated

☆ Research approved by the Institutional Review Board (IRB) of the University of Southern California and supported by the Reorganizational Living Foundation.

* Corresponding author at: 3740 McClintock Avenue, Room EEB 306, Los Angeles, CA 90089-2563, United States.
E-mail addresses: mart737@usc.edu (R. Martin del Campo), jonckhee@usc.edu (E. Jonckheere).
URL: http://eudoxus2.usc.edu (E. Jonckheere).

http://dx.doi.org/10.1016/j.bspc.2016.08.011
1746-8094/

with a CPG, can undergo "bifurcations," here understood in a signal processing sense with a view towards the period-halving dynamical interpretation [7]. Finally, another contribution is to show how to deal with signals less than ideal, as those of [1] were.

1.2.1. Reproducibility (Case Study I)

Nearly 10 years separate the data collection upon which [1] is based from the present one. During that time, the entrainment technique evolved to make the movement better controllable (the sEMG signals can be made smooth or bursty at will), the electrode positioning underwent some slight changes while we experienced with different orientation of the differential amplifier input prongs relative to muscle fibers, and the hardware (front-end electronics together with sEMG amplifiers) was upgraded. The software underwent some upgrade as well. Despite these changes and a 10-year span between the two experiments, we show in "Case Study I" that the early results [1] upon which the CPG hypothesis rests are reproducible.

1.2.2. Bifurcation (Case Study II)

In Case Study II, we add another attribute that can be associated with a CPG: the ability to undergo "bifurcations." The early clues that pointed to such phenomena were visually obvious discontinuities in the sEMG signal, as Fig. 5 shows. More formally, here, bifurcation is defined as qualitative structural change; more specifically in the context of the *standing wave* CPG, bifurcation is typically a change in the mode shape, concomitant with a change in the frequency of the coherent oscillations. From a signal processing view point, this amounts to a shift in the cross power spectral density of the signals at a distance, something that we endeavored to confirm with inferential statistics. Another sign of this bifurcation phenomenon is a shift of the coherent oscillations from the D_8 to the D_7 subbands of the DB3 wavelet decomposition. As the difference between D_8 and D_7 is a matter of time scale, this is certainly consistent with the shift of the mean in the cross spectral densities confirmed by statistical tests of hypothesis.

In the topological and qualitative classifications of [8], our definition of "bifurcation" rather matches a "qualitative" trait of [8]. In the dynamical sense, our bifurcation is a period-halving phenomenon [7], so that it has some of the attributes of a topological bifurcation.

Existence of bifurcations should not be that surprising for such a complex system as the human spinal neuro-skeletal system. It simply cannot be expected to oscillate at a single eigenmode and such factors as breathing, even thought processes, have the potential to change the oscillation structural properties. Many such bifurcations on other subjects have already been observed [9,10] using different methods though. In particular, another bifurcation from 1 to 2 mode shape nodes was already confirmed using ARIMA modeling [9] of the SAS statistical package.

1.2.3. Less than ideal signals

In the case the signals are analyzed across a bifurcation, the correlation pattern that reveals coherence cannot be expected to be as crisp as that of the ideal, "textbook" example of [1]. As such, another purpose of Case Study II of the present paper is to assess by how much the correlation pattern deviates from that of [1] when conditions are no longer ideal.

2. Methods

The control subjects of the two case-studies presented here are both healthy individuals who, prior to recordings, had signed the informed consent form approved by the Institutional Review Board (IRB) of the University of Southern California. Surface Electromyography (sEMG) reduced-noise tripolar electrodes were placed at

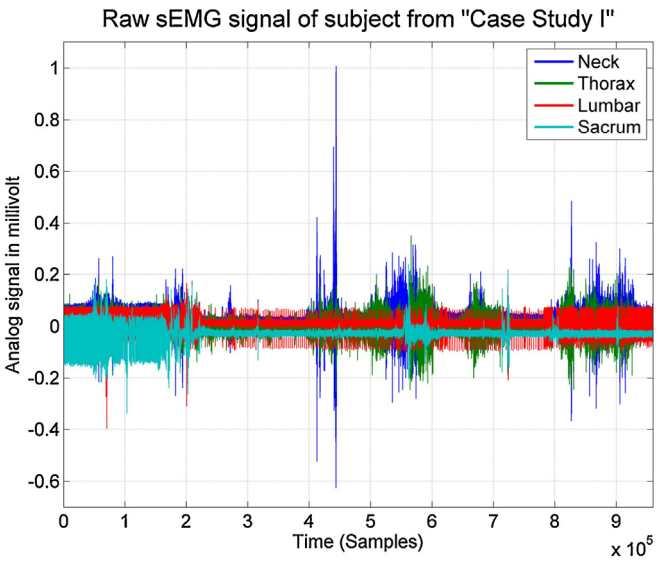

Fig. 1. Raw sEMG data at cervical, thoracic, lumbar and sacral positions of Case Study I.

cervical (C2-C3), thoracic (T4-T6), lumbar (L3), and sacral (S2-S4) positions. The sensitive input prongs of the front-end electronics were aligned with the back muscle fibers [11]. The sEMG signals were amplified by an Insight Subluxation Station, Discovery model. The analog-to-digital conversion was done by a USB-1608FS card manufactured by Measurement Computing™ and running on a Windows XP platform.

During Case Study I, 960,000 sample points of sEMG activity were recorded at a rate of 4 kHz as shown in Fig. 1. The analysis was performed during the first 120,000 samples because there is visual evidence that the signals burst synchronously at the beginning of the recording; this data segment is amplified in Fig. 2. This phenomenon of synchronicity of sEMG signals has also been observed on a different research subject [12].

The procedure for Case Study II was similar. Three seconds of data were analyzed using the same sampling rate as Case Study I. This data segment comprises a set of 12,000 samples, in which the bifurcation is present, as shown in Fig. 5.

We highlight the differences between the protocol of the earlier study [1] and the protocol utilized to collect the data of Case-Studies

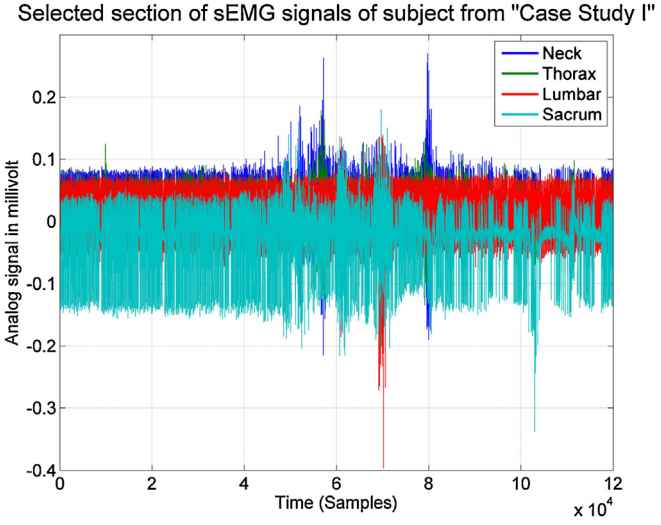

Fig. 2. Segment of first 120,000 samples from Case Study I at cervical, thoracic, lumbar and sacral positions.

I and II. First, in the earlier study, the sensitive prongs of the electrode front-end electronics were put at a 45° angle relative to spine, whereas in the present study they were aligned with the skeletal muscle fibers. Second, the sacral electrode had been positioned on the gluteus, as opposed to the sacrum as reported here. Third, the sEMG signals had been previously amplified by an older Insight Millennium sEMG machine and the analog-to-digital conversion done with an older PC-Card DAS16/16, manufactured by Computer Boards (now Measurement Computing™, running on a Windows 98 operating system.

The fundamental tool in the sEMG signal analysis is the Daubechies DB3 wavelet decomposition. This wavelet is chosen because its mother function mimics the single motor unit action potential. Besides, it was found that the D_7 and D_8 subbands of the DB3 offer the best spatial correlation properties among the signals recorded on the spine. Probably most importantly, as seen from Figure 2 of [1], the D_7 and D_8 subbands of the DB3 wavelet decomposition reveal the electrophysiology specific "synchronization doublets" [2,13] contributing to the coherence. On the other hand, the D_7 and D_8 subband signals in a different Daubechies wavelet order, such as DB2, do not show the resonant-type doublets [13] as clearly as those on the DB3.

Let $y_1(k), y_2(k), y_3(k), y_4(k)$ be either the D_8 or the D_7 subband of the cervical, thoracic, lumbar and sacral signals, resp., sEMG signals. As in [1], we define the empirical correlations

$$r_{ij}(s) = \frac{\sum_{k=1}^{K-s}(y_i(k)-\bar{y}_i)(y_j(k+s)-\bar{y}_j)}{\sqrt{\sum_{k=1}^{K-s}(y_i(k)-\bar{y}_i)^2}\sqrt{\sum_{k=1}^{K-s}(y_j(k)-\bar{y}_j)^2}}.$$

As argued in [1], the movement has a coherent standing wave if there exist some delays $s_1 < s_2 < \ldots$ such that

$$r_{ij}(s_\ell) = 0; \quad i,j = 1,2,3,4; \quad \ell = 1,2,\ldots$$

The points s_ℓ, ℓ=1, 2, . . ., have been called *zero correlation nodes* and are manifestations of a coherent standing wave. Clearly, one cannot expect a perfectly coherent standing wave and the above will not, in general, hold for all ℓ's. In practice, one can expect the above to hold reasonably accurately for ℓ=1; the accuracy already deteriorates for ℓ=2, and we never observed a convincing zero correlation node of order ℓ>3.

3. Results: reproducibility: Case Study I

Eyeball inspection of the raw sEMG traces in Fig. 1 already shows some coherence as there is evidence that the signals are bursting synchronously. In a similar way as in [12], but with a different subject, we selected a segment of data for analysis, the first 120,000 samples, which besides having synchronous signals between samples 50,000 and 80,000 also has a sub-segment where the synchronous bursting is not visually obvious—before sample 50,000. The analyzed segment of 120,000 samples of raw signal is plotted in Fig. 2.

Note that the signals of Fig. 2 are slightly more bursty than that of Figure 1 of [1], and less bursty than those of Figure 2 of [12]. Nevertheless, the coherence results *remain qualitatively the same*.

The 1-D wavelet transform [14] was utilized for noise reduction at the 8th decomposition level. The transform is computed using the Mallat's algorithm [15], which has a pyramidal filtering scheme with a set of consecutive low and high pass filters, determined according to the Daubechies-3 mother wavelet function (DB3) [16], followed by a decimation (down-sampling) by a factor of 2. The decomposition of the raw signal results into different scales considered to be distinct frequency subbands, and the idea is to clean out "unimportant" subbands considered to be noise. As argued in [5], the signals in the D_1 to D_5 subbands are not of interest because

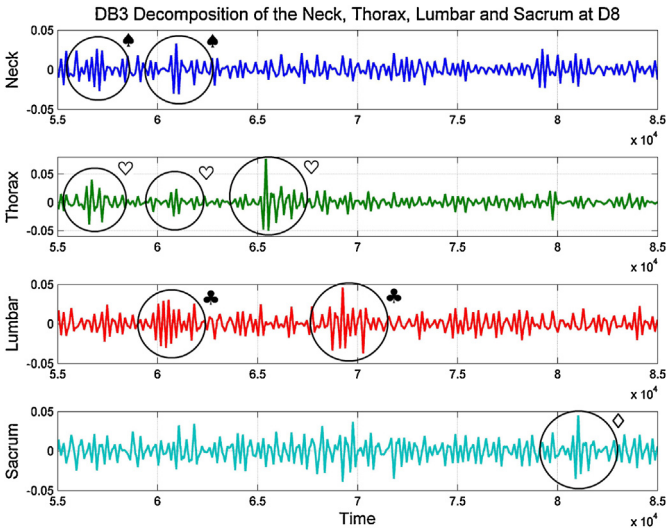

Fig. 3. D_8 subband signals of the Daubechies DB3 wavelet decomposition at the cervical, thoracic, lumbar and sacral positions, respectively.

they consist primarily of high frequency noise, whereas the D_7 and D_8 components show more clearly the "wavelet packets," and D_8 exhibits the better correlation properties. Furthermore, the D_8 subband signals offer the most sizable difference between a voluntary, fake motion and the spinal wave movement [1].

A summary of the D_8 subbands of the neck to sacrum signals is shown in Fig. 3. Most importantly, observe—quite consistently with Figure 2 of [1]—the synchronization doublets of the cervical, thoracic, lumbar and sacral signals marked with a circle and identified with a spade suit symbol ♠, a heart suit symbol ♡, a club suit symbol ♣, and a diamond suit symbol ♢, respectively.

Note, also consistently with [1], that the bursts on the raw signal also occur when the D_8 subband signals show doublets. It is important to undersocre, however, that the bursts in the raw signal around samples 60,000 and 70,000 span longer than the mild bursts of the raw signal in Figure 1 of [1], and thus the doublets are less perceivable.

The cross-correlations between pairs of D_8 subbands of the sEMG signals are shown in Fig. 4.

The plots of Fig. 4a–d are quite similar to those of the left panels of Figures 3–6 of [1]. The s_1 zero correlation nodes (marked with black circles) develop with a higher level of accuracy than in [1], while the s_2 nodes (marked with dotted circles) can be seen, but not as markedly as the s_1 nodes, but still with a higher accuracy than the s_2 nodes of [1].

4. Results: zero correlation nodes across bifurcation: Case Study II

The raw sEMG data recorded for this case study is shown in Fig. 5 for neck and thorax signals.

Between samples 4300 and 5300, the upper spine signals exhibit a clear discontinuity. Remarkably, this discontinuity in the sEMG traces occurred *exactly* at the time the practitioner, who had no visual contact with the real-time oscilloscopic display of the sEMG signals, called a visually observable change in the structural properties of the spinal wave. (The discontinuity in the lower spine signals is not visually obvious, but is confirmed by the analysis of Section 5.)

The analysis is broken down in two parts: first, "before the bifurcation," i.e., from sample 1 until sample 4000; second, "after the bifurcation," that is, between sample 5411 and sample 9871. Thus, the specific segment that comprises the bifurcation, namely, between samples 4300 and 5300, is deliberately avoided, because

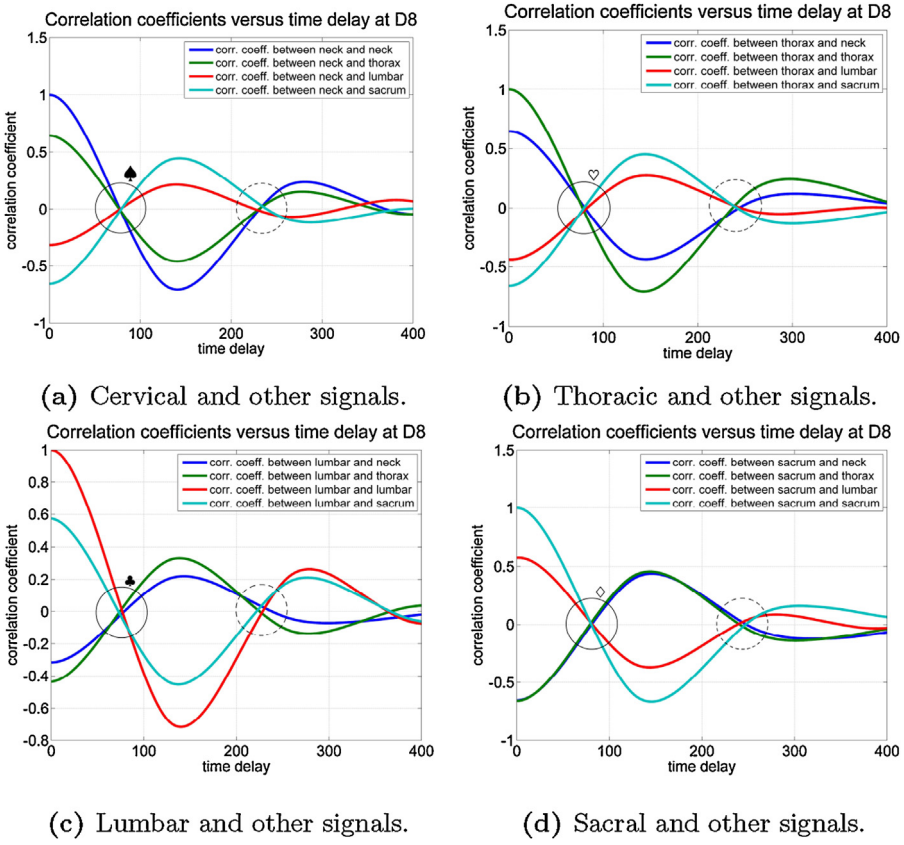

Fig. 4. Correlation between D_8 subbands of top to bottom spine signals during the first 120,000 samples for "Case Study I" subject.

the standing wave momentarily disappears and the signals are no longer stationary.

4.1. Analysis before bifurcation

The specificity of the sEMG signals is observed on the relevant D_6, D_7 and D_8 subbands of the DB3 wavelet decomposition, as it is shown in Figs. 6–8. The cases of synchronization doublets consistent with zero correlation nodes are identified with circles.

The correlation plots of the D_6, D_7, D_8 subbands before the bifurcation are shown in Figs. 9–11, respectively. The thoracic correlation plot (Fig. 9b) does not show coherence at the D_8 subband, in contrast with the other three signals. Complementary to this observation, the correlation of the thorax is at the D_7 subband, which exhibits a better defined zero correlation node as shown in Fig. 10b and labeled with a triangle △. The sacral curve shows some aberration because of the sacral electrode positioning (not the same as that of [1].) On the D_7, not much correlation can be seen, except for the thoracic plot. On the D_6, not much correlation can be seen.

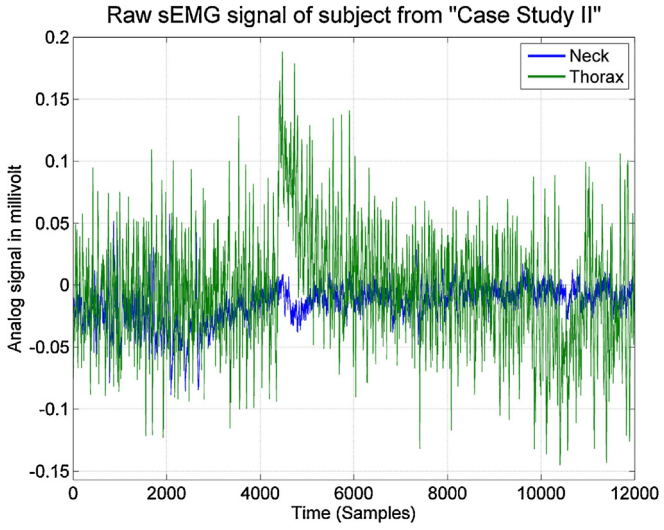

Fig. 5. Raw sEMG cervical and thoracic signals for "Case Study II" subject.

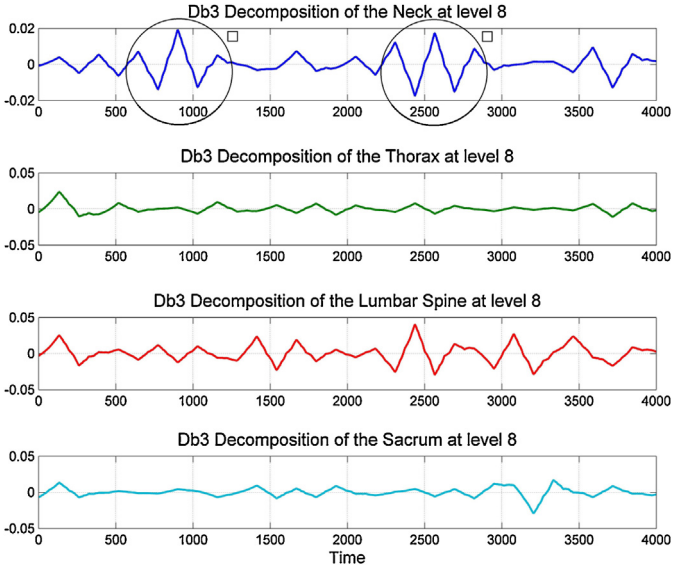

Fig. 6. D_8 subband signals of DB3 decomposition of top to bottom spine signals before bifurcation for "Case Study II" subject.

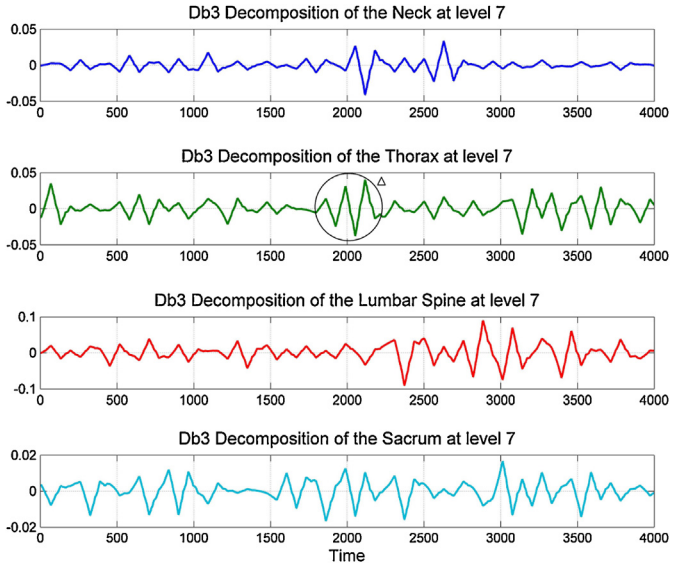

Fig. 7. D_7 subband signals of DB3 decomposition of top to bottom spine signals before bifurcation for "Case Study II" subject.

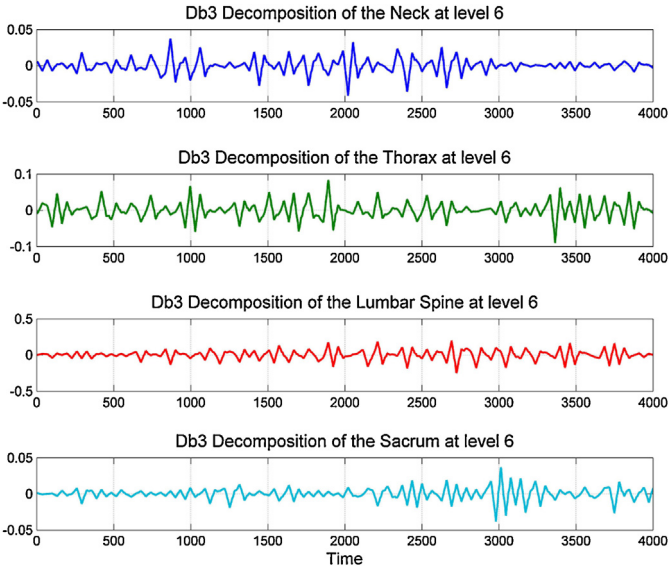

Fig. 8. D_6 subband signals of DB3 decomposition of top to bottom spine signals before bifurcation for "Case Study II" subject.

(On the lumbar plots, there *appears* to be a crossing, but it is too far off the $r = 0$ axis to be of any significance.)

4.2. Analysis after bifurcation

The same procedure was performed after the data segment where the bifurcation phenomenon terminates, and involves approximately 1 s of sEMG trace (from 5411 to 9871 samples). As in the previous case (before the bifurcation), the wavelet packets were best observed on the D_6, D_7 and D_8 subbands. The corresponding correlation plots after the bifurcation are shown in Figs. 12–14. On the D_8 subband, not much correlation can be seen, except possibly on the sacral curves (see black circle). On the other hand, the D_7 subband shows several s_1 nodes and even higher order zero correlation nodes (see dotted circles). The D_6 does not appear to show any zero correlation nodes.

5. Results: shift in cross spectral density: Case Study II

It can be observed in Figs. 9, 10, 12 and 13 that the "slow" D_8 sub-band shows larger correlation than the D_7 sub-band *before the bifurcation*, and the "faster" D_7 sub-band shows larger correlation

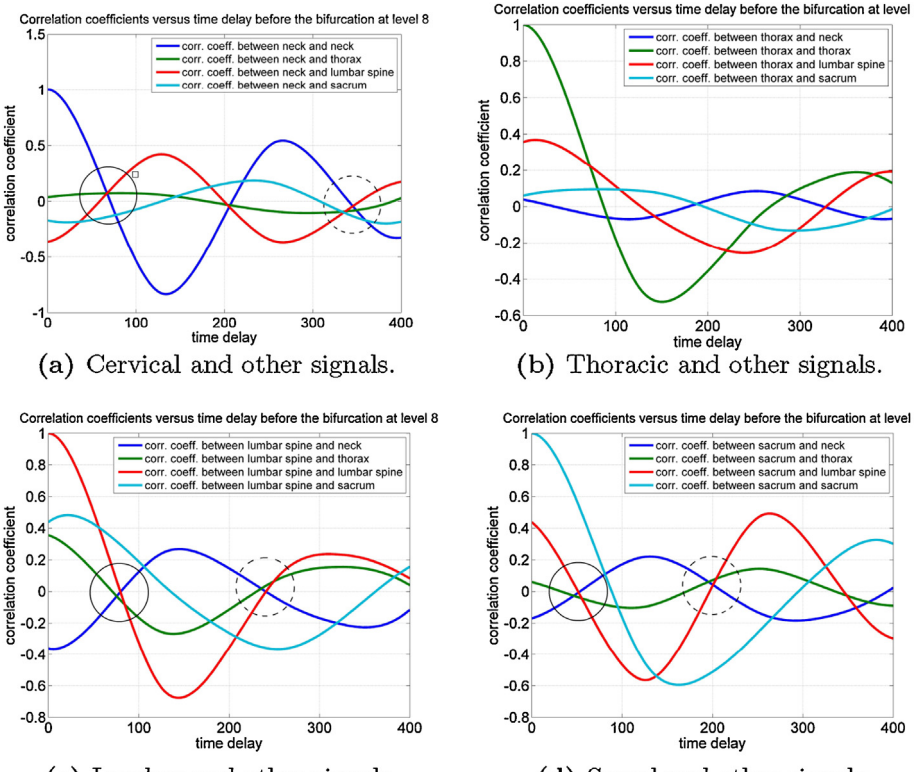

Fig. 9. Correlation between D_8 subbands of top to bottom spine signals before bifurcation for "Case Study II" subject.

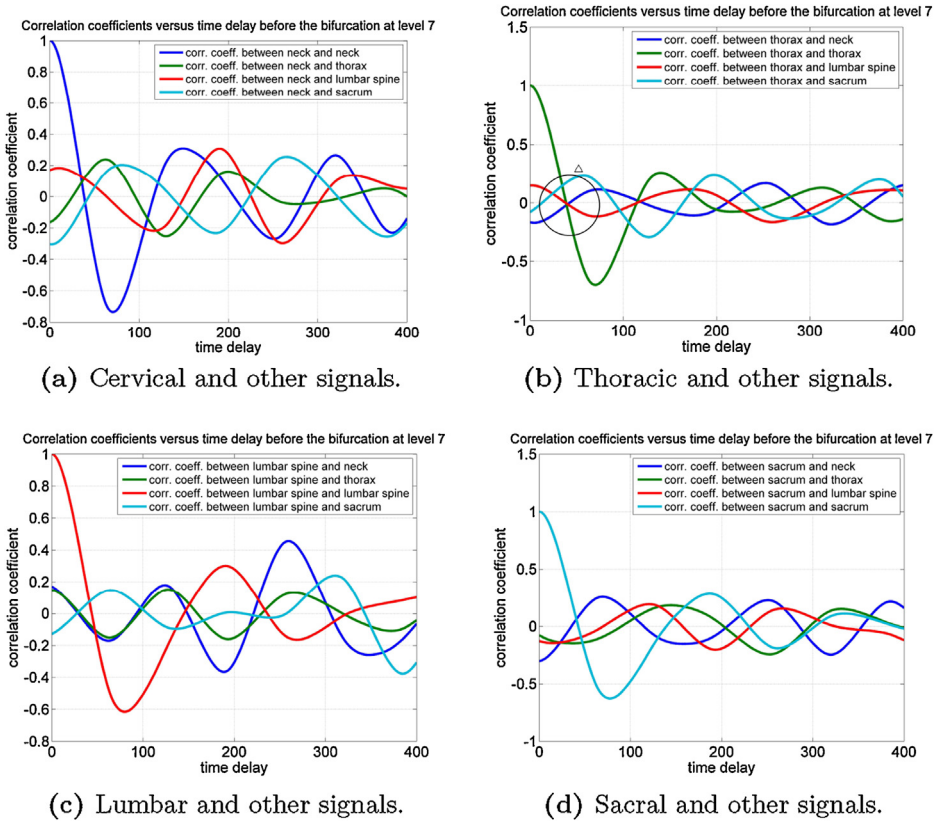

Fig. 10. Correlation between D_7 subbands of top to bottom spine signals before bifurcation for "Case Study II" subject.

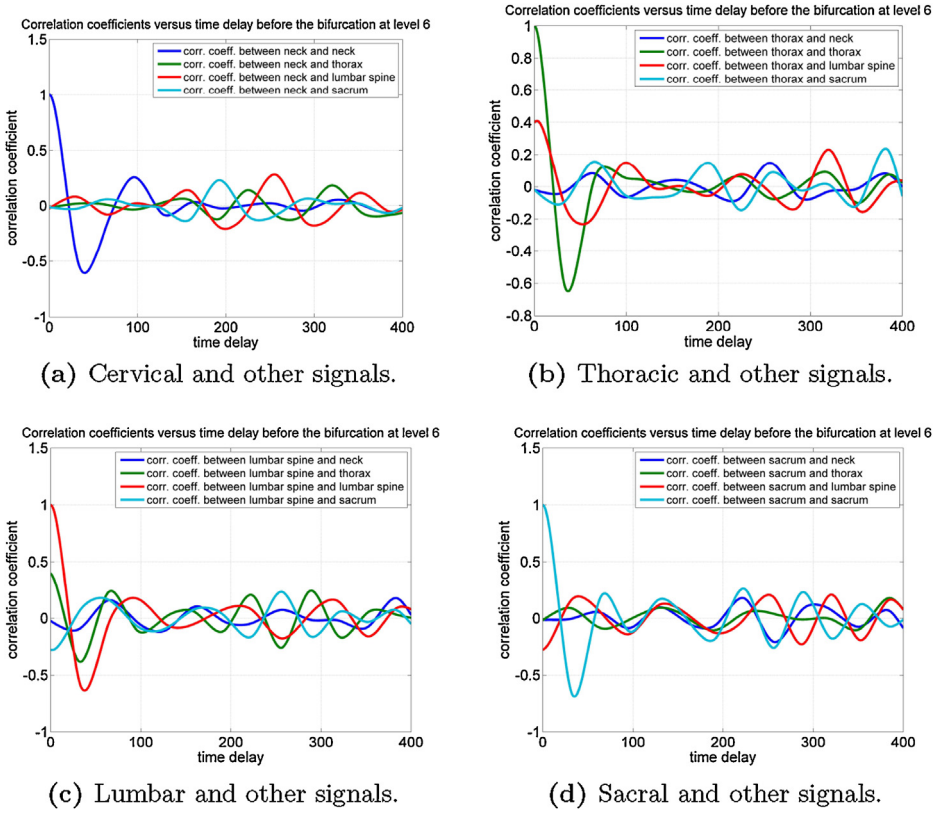

Fig. 11. Correlation between D_6 subbands of top to bottom spine signals before bifurcation for "Case Study II" subject.

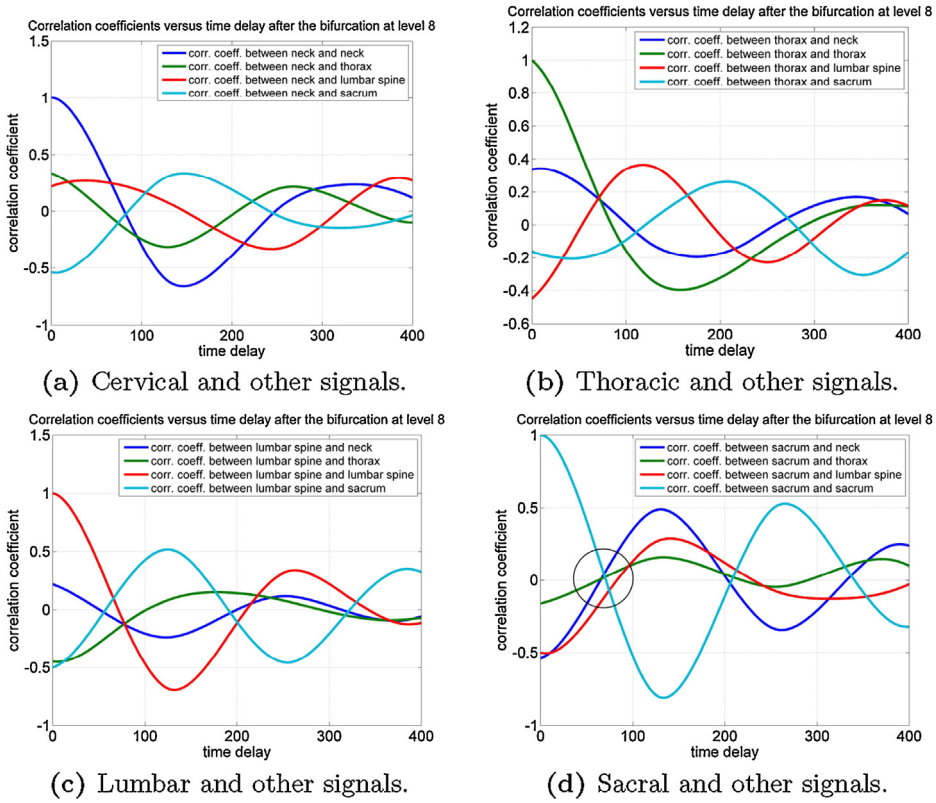

Fig. 12. Correlation between D_8 subbands of top to bottom spine signals after bifurcation for "Case Study II" subject.

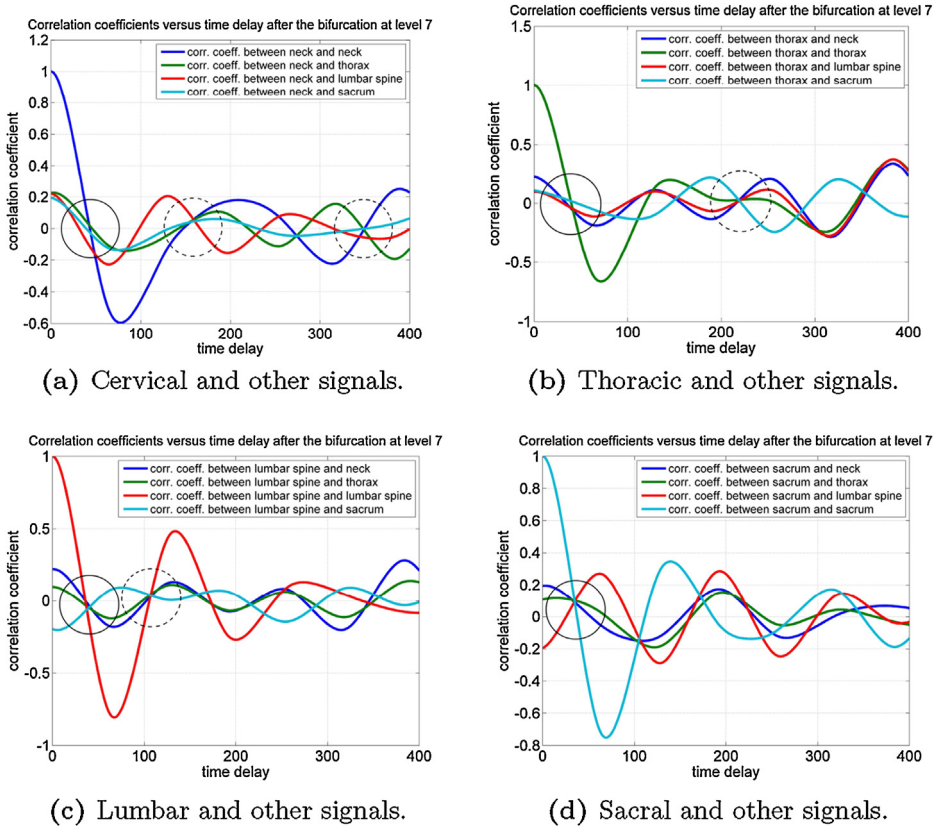

Fig. 13. Correlation between D_7 subbands of top to bottom spine signals after bifurcation for "Case Study II" subject.

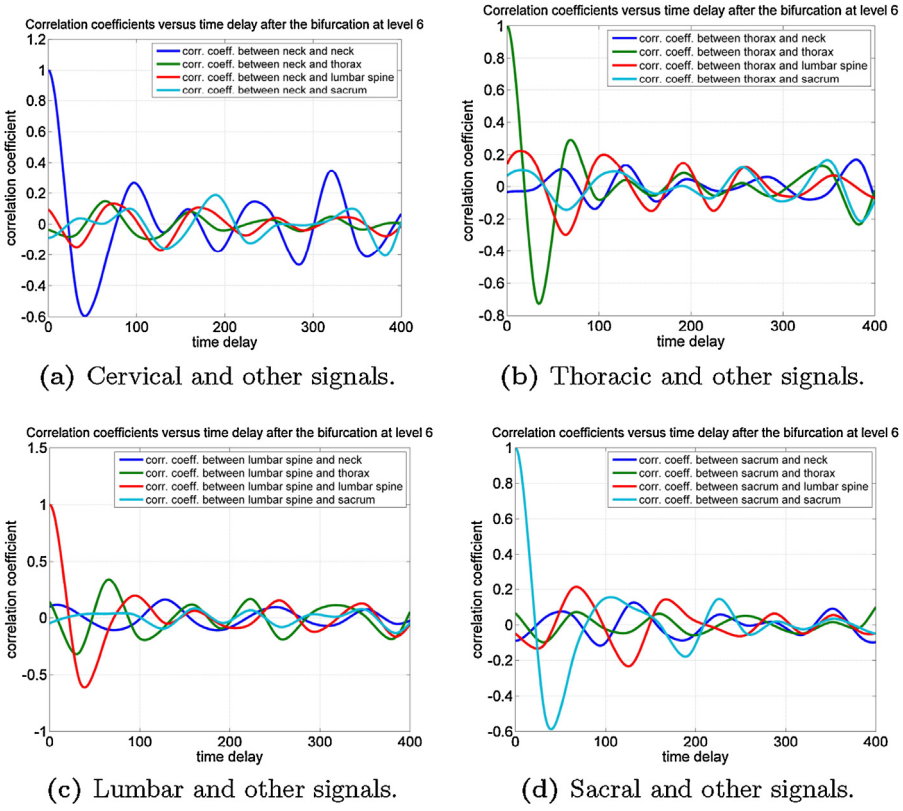

Fig. 14. Correlation between D_6 subbands of top to bottom spine signals after bifurcation for "Case Study II" subject.

than the D_8 sub-band *after the bifurcation*. Thus, we expect the *cross Power Spectral Density (cPSD)* between two signals along the spine to be larger in high frequency *after the bifurcation*. Equivalently, we expect the *cPSD* to be larger in low frequency *before the bifurcation*. It is the purpose of this section to show that this "educated guess" is supported by the data from the lower spinal signals and is confirmed by a statistical test of significance.

After obtaining the cPSD of the spine signals, that is, the frequency distribution of the 16 possible cases of correlation between two signals out of the four (cervical, thoracic, lumbar, and sacral) spine signals, we come up with a *qualitative* behavior of the cPSD across the bifurcation for the lower spine signals as shown in Fig. 15. The randomness is analyzed in terms of the normalized cPSD distributions, and we define the "Before" and "After" probability density functions, $f_P^B(\rho)$, $f_P^A(\rho)$, respectively. Let μ_P^B, μ_P^A be the means of $f_P^B(\rho)$, $f_P^A(\rho)$, respectively. To statistically demonstrate the existence of the intersection between the red and blue curves of Fig. 15, the test was broken down into low normalized frequencies, from 0 to 0.5, and high normalized frequencies, from 0.51 to 1. From this standpoint, it suffices to show that, statistically, there is enough confidence in asserting that $\mu_P^B < \mu_P^A$ at high frequencies and $\mu_P^B > \mu_P^A$ at low frequencies.

5.1. Prelude: test of significance under Gauss assumption

Since we focus our attention on the randomness defined by the cPSD values, we statistically define $\rho_1^B, \rho_2^B, \rho_3^B, \ldots, \rho_m^B$ as a random draw from $f_P^B(\rho)$ and $\rho_1^A, \rho_2^A, \rho_3^A, \ldots, \rho_m^A$ as a random draw from $f_P^A(\rho)$. Define the "Before" and "After" means as

$$\bar{\rho}^B = \frac{1}{m}\sum_{i=1}^{m}\rho_i^B, \quad \bar{\rho}^A = \frac{1}{m}\sum_{i=1}^{m}\rho_i^A.$$

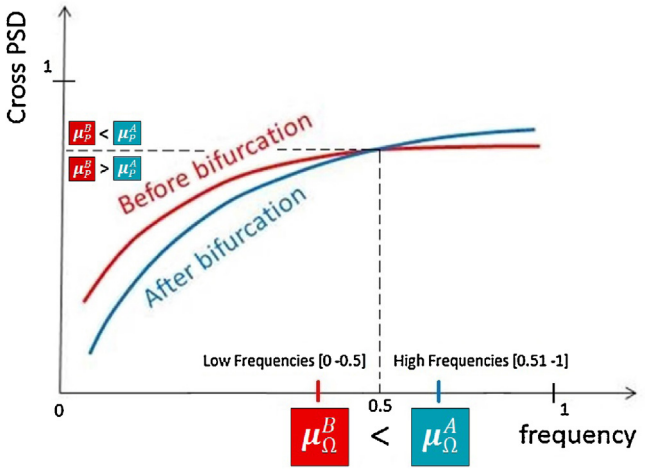

Fig. 15. Qualitative behavior of the cross power spectral densities (cPSDs) for signals *Before* (red) and *After* (blue) bifurcation. (For interpretation of the references to color in this figure legend, the reader is referred to the web version of the article.)

Define the sample variances:

$$(s^B)^2 = \frac{1}{m-1}\sum_{i=1}^{m}(\rho_i^B - \bar{\rho}^B)^2, \quad (s^A)^2 = \frac{1}{m-1}\sum_{i=1}^{m}(\rho_i^A - \bar{\rho}^A)^2.$$

It turns out that, under Gauss assumption on the normalized cPSDs, $f_P^B(\rho)$ and $f_P^A(\rho)$, the quantity

$$t = \frac{\bar{\rho}^B - \bar{\rho}^A}{\sqrt{\frac{(s^B)^2 + (s^A)^2}{m}}}$$

Table 1
p-Values of bootstrap statistical test from upper spine signals.

Upper Spine Signals					
Neck	Neck & Neck BEFORE VS AFTER				
	Frequencies	Alternative Hypothesis	P-values calculated using: MatLab	JMP	Conclusion
	Low	$Ha: \mu_{Before} > \mu_{After}$	0.97185 (S.D. = 0.000212)	0.97	Fail to reject H_0
	High	$Ha: \mu_{Before} < \mu_{After}$	0.99925 (S.D. = 0.0000527)	0.9986	Fail to reject H_0
	Neck & Thorax BEFORE VS AFTER				
	Frequencies	Alternative Hypothesis	P-values calculated using: MatLab	JMP	Conclusion
	Low	$Ha: \mu_{Before} > \mu_{After}$	0.9149 (S.D. = 0.000270801)	0.9139	Fail to reject H_0
	High	$Ha: \mu_{Before} < \mu_{After}$	0.43112 (S.D. = 0.000332666)	0.4322	Fail to reject H_0
	Neck & Lumbar BEFORE VS AFTER				
	Frequencies	Alternative Hypothesis	P-values calculated using: MatLab	JMP	Conclusion
	Low	$Ha: \mu_{Before} > \mu_{After}$	0.95266 (S.D. = 0.000117379)	0.9544	Fail to reject H_0
	High	$Ha: \mu_{Before} < \mu_{After}$	1.0000 (S.D. = 0.0000)	0.9999	Fail to reject H_0
	Neck & Sacrum BEFORE VS AFTER				
	Frequencies	Alternative Hypothesis	P-values calculated using: MatLab	JMP	Conclusion
	Low	$Ha: \mu_{Before} > \mu_{After}$	0.00332 (S.D. = 0.00004216)	0.0030	Reject H_0
	High	$Ha: \mu_{Before} < \mu_{After}$	0.00199 (S.D. = 0.00005676)	0.002	Reject H_0
Thorax	Thorax & Neck BEFORE VS AFTER				
	Frequencies	Alternative Hypothesis	P-values calculated using: MatLab	JMP	Conclusion
	Low	$Ha: \mu_{Before} > \mu_{After}$	0.91496 (S.D. = 0.0002319)	0.9139	Fail to reject H_0
	High	$Ha: \mu_{Before} < \mu_{After}$	0.4311 (S.D. = 0.000505525)	0.4322	Fail to reject H_0
	Thorax & Thorax BEFORE VS AFTER				
	Frequencies	Alternative Hypothesis	P-values calculated using: MatLab	JMP	Conclusion
	Low	$Ha: \mu_{Before} > \mu_{After}$	0.92745 (S.D. = 0.000236878)	0.9275	Fail to reject H_0
	High	$Ha: \mu_{Before} < \mu_{After}$	0.05179 (S.D. = 0.000172884)	0.0517	Fail to reject H_0
	Thorax & Lumbar BEFORE VS AFTER				
	Frequencies	Alternative Hypothesis	P-values calculated using: MatLab	JMP	Conclusion
	Low	$Ha: \mu_{Before} > \mu_{After}$	0.42737 (S.D. = 0.000386005)	0.4271	Fail to reject H_0
	High	$Ha: \mu_{Before} < \mu_{After}$	0.0000 (S.D. = 0.0000)	0.0001	Reject H_0
	Thorax & Sacrum BEFORE VS AFTER				
	Frequencies	Alternative Hypothesis	P-values calculated using: MatLab	JMP	Conclusion
	Low	$Ha: \mu_{Before} > \mu_{After}$	0.0000 (S.D. = 0.0000)	0.0001	Reject H_0
	High	$Ha: \mu_{Before} < \mu_{After}$	1.0000 (S.D. = 0.0000)	0.9999	Fail to reject H_0

has approximately a *t*-distribution [17], and becomes Gaussian for m large. We want to show that $\mu_P^B < \mu_P^A$ for f_P^B, f_P^A restricted to high frequencies and $\mu_P^B > \mu_P^A$ for distributions restricted to low frequencies.

The problem is that the Shapiro–Wilk W test of goodness-of-fit has shown that $f_P^B(\rho)$, $f_P^A(\rho)$ *do not* follow the Gauss distribution. Thus, to go around the lack of Gaussian property of $f_P^B(\rho)$, $f_P^A(\rho)$, we need to perform bootstrapping of the cPSD values.

5.2. No Gauss assumption: bootstrapping

Bootstrapping is a Monte Carlo method [18] that employs repeated samples with replacement from the original data. This testing procedure is useful when the theoretical distribution of the statistic is complicated or unknown. Using bootstrapping, we conducted a statistical test of hypothesis to estimate the Achieved Significance Level (ASL) of the test, also known as *p-value*.

Table 2
p-Values of bootstrap statistical test from lower spine signals.

Lower Spine Signals					
Lumbar	Lumbar & Neck BEFORE VS AFTER				
	Frequencies	Alternative Hypothesis	P-values calculated using: MatLab	P-values calculated using: JMP	Conclusion
	Low	$Ha: \mu_{Before} > \mu_{After}$	0.04732 (S.D. = 0.000297396)	0.0456	Reject H_0
	High	$Ha: \mu_{Before} < \mu_{After}$	1.0000 (S.D. = 0.0000)	0.9999	Fail to reject H_0
	Lumbar & Thorax BEFORE VS AFTER				
	Frequencies	Alternative Hypothesis	P-values calculated using: MatLab	P-values calculated using: JMP	Conclusion
	Low	$Ha: \mu_{Before} > \mu_{After}$	0.42693 (S.D. = 0.000678315)	0.4271	Fail to reject H_0
	High	$Ha: \mu_{Before} < \mu_{After}$	0.0000 (S.D. = 0.0000)	0.0001	Reject H_0
	Lumbar & Lumbar BEFORE VS AFTER				
	Frequencies	Alternative Hypothesis	P-values calculated using: MatLab	P-values calculated using: JMP	Conclusion
	Low	$Ha: \mu_{Before} > \mu_{After}$	0.00265 (S.D. = 0.000052704)	0.0025	Reject H_0
	High	$Ha: \mu_{Before} < \mu_{After}$	0.0000 (S.D. = 0.0000)	0.0001	Reject H_0
	Lumbar & Sacrum BEFORE VS AFTER				
	Frequencies	Alternative Hypothesis	P-values calculated using: MatLab	P-values calculated using: JMP	Conclusion
	Low	$Ha: \mu_{Before} > \mu_{After}$	0.0000 (S.D. = 0.0000)	0.0001	Reject H_0
	High	$Ha: \mu_{Before} < \mu_{After}$	0.9967 (S.D. = 0.0000816497)	0.9966	Fail to reject H_0
Sacrum	Sacrum & Neck BEFORE VS AFTER				
	Frequencies	Alternative Hypothesis	P-values calculated using: MatLab	P-values calculated using: JMP	Conclusion
	Low	$Ha: \mu_{Before} > \mu_{After}$	0.00331 (S.D. = 0.000073786)	0.0030	Reject H_0
	High	$Ha: \mu_{Before} < \mu_{After}$	0.002 (S.D. = 0.0000471405)	0.002	Reject H_0
	Sacrum & Thorax BEFORE VS AFTER				
	Frequencies	Alternative Hypothesis	P-values calculated using: MatLab	P-values calculated using: JMP	Conclusion
	Low	$Ha: \mu_{Before} > \mu_{After}$	0.0000 (S.D. = 0.0000)	0.0001	Reject H_0
	High	$Ha: \mu_{Before} < \mu_{After}$	1.0000 (S.D. = 0.0000)	0.9999	Fail to reject H_0
	Sacrum & Lumbar BEFORE VS AFTER				
	Frequencies	Alternative Hypothesis	P-values calculated using: MatLab	P-values calculated using: JMP	Conclusion
	Low	$Ha: \mu_{Before} > \mu_{After}$	0.0000 (S.D. = 0.0000)	0.0001	Reject H_0
	High	$Ha: \mu_{Before} < \mu_{After}$	0.99671 (S.D. = 0.000031622)	0.9966	Fail to reject H_0
	Sacrum & Sacrum BEFORE VS AFTER				
	Frequencies	Alternative Hypothesis	P-values calculated using: MatLab	P-values calculated using: JMP	Conclusion
	Low	$Ha: \mu_{Before} > \mu_{After}$	0.0000 (S.D. = 0.0000)	0.0001	Reject H_0
	High	$Ha: \mu_{Before} < \mu_{After}$	1.0000 (S.D. = 0.0000)	0.9999	Fail to reject H_0

We begin by calculating the value of the test statistic for the sample:

$$t_{\text{calc}} = \frac{\bar{\rho}^B - \bar{\rho}^A}{\sqrt{\frac{(s^B)^2 + (s^A)^2}{m}}}.$$

Then we transform the m values from the B-sample as $x_i^B = \rho_i^B - \bar{\rho}^B + \bar{\bar{\rho}}$ and those from the A-sample as $x_i^A = \rho_i^A - \bar{\rho}^A + \bar{\bar{\rho}}$, where $\bar{\bar{\rho}} = (\bar{\rho}^B + \bar{\rho}^A)/2$ is the mean of the combined samples; thereafter, we randomly sample $\{x_i^A\}$ and $\{x_i^B\}$ with replacement and repeat the same operation a total of j times.

For each bootstrap sample j, we compute the test statistic

$$t_j = \frac{\bar{x}^B - \bar{x}^A}{\sqrt{\frac{(s^B)^2 + (s^A)^2}{m}}},$$

where $\bar{x}^B$ and $\bar{x}^A$ are the means of bootstrap sample j for sample $\{x_i^B\}$ and $\{x_i^A\}$, respectively.

Next, we define the *Null Hypothesis* H_0 as follows:

$$H_0 : (\mu_P^B - \mu_P^A) = 0,$$

and we define the *Alternative Hypotheses* and the bootstrap estimated *p-value* as

$$\text{Upper-tailed test}\,(H_a : (\mu_P^B - \mu_P^A) > 0): \quad \text{ASL} = \frac{\text{Number of times } t_j > t_{\text{calc}}}{j}$$

$$\text{Lower-tailed test}\,(H_a : (\mu_P^B - \mu_P^A) < 0): \quad \text{ASL} = \frac{\text{Number of times } t_j < t_{\text{calc}}}{j}$$

"Upper-tailed" ("Lower-tailed") test refers to low (high) frequency restrictions of f_P^B, f_P^A.

The bootstrapping procedure described above was implemented on MatLab, and it was run at least ten times for each of the $j = 100, j = 1,000, j = 10,000, j = 100,000$, and $j = 1,000,000$ bootstrap samples from the cPSD of every pair of signals at low and high frequencies. The averages of the *p*-values and their convergence to a stable value for every j is shown in Appendix section of the *Technical Report* [19]. In addition, this bootstrap analysis was also run on JMP Pro 11, a statistical software developed by the SAS Institute. Using $j = 10,000$ on JMP Pro 11 we obtained similar *p*-values as those on the MatLab bootstrap analysis. Both *p*-values are reported in Tables 1 and 2.

We reject the Null Hypothesis when the *p*-values fall below a significance level of $\alpha = 0.05$. In Tables 1 and 2, we highlight those cases that significantly concur with the qualitative behavior gleaned from Fig. 15. Clearly, the Alternative Hypothesis holds in just about all cases involving lower spine signals (Table 2), whereas the Alternative Hypothesis is a bit problematic for the upper spine signals (Table 1). This explanation is that the sacral oscillator as shown in [1, Figure 8] is better engaged that the cervical one.

6. Discussion: reproducibility: Case Study I

Observe in Fig. 4 the well-defined "zero correlation nodes," i.e., the common points of intersection of all the $r_{ij}(s)$ versus s curves and the $r = 0$ axis, strong evidence of a coherent standing wave. Both the s_1 nodes and to a less extent the s_2 nodes are visible (marked with solid and dotted circles, resp.). Also note the consistency between the cervical synchronization doublets in Fig. 3 and the s_1 node of Fig. 4a, both identified with spade suit symbols ♠; the thoracic synchronization doublets in Fig. 3 and the s_1 node of Fig. 4b, both identified with heart suit symbols ♡; the lumbar synchronization doublets in Fig. 3 and the s_1 node of Fig. 4c, both identified with club suit symbols ♣; the sacral synchronization doublet in Fig. 3 and the s_1 node of Fig. 4d, both identified with diamond suit symbols ♢. As such, it is fair to say that the results of [1] have been reproduced in an environment deliberately taken not as "clean" as that of [1].

However, the same results are not as visually obvious for Case Study II when a "bifurcation" occurs.

7. Discussion: bifurcation: Case Study II

Before the bifurcation, the "zero correlation nodes" are somehow clear on the D_8 subband as shown in Fig. 9, but markedly depleted on the D_7 and D_6 subbands, as shown in Figs. 10 and 11, respectively.

Observe the consistency between the synchronization doublets of Fig. 6 and the s_1 node of Fig. 9a, marked with a box □. We have the same consistency between the synchronization doublets of Fig. 7 and the s_1 node of Fig. 10b, marked with a triangle △.

After the bifurcation, the D_8 subband is no longer the best to reveal coherence as shown in Fig. 12a–d. Contrarily to [1] and Case Study I of the present paper, the D_7 subband of the signals restricted from sample 5411 to 9871 exhibits better zero correlation nodes as shown in Fig. 13a–d.

The qualitative behavior of Fig. 15 happens to be consistent for the lower spinal signals, as demonstrated by the statistical test of significance, where a depletion of the low frequency component occurs predominantly *after the bifurcation*. Furthermore, this statistical test corroborates the zero correlation nodes pattern that takes place on two different subbands when the system passes through a bifurcation.

It is thus fair to say that, before the bifurcation, the coherence is at the D_8 level, while, after the bifurcation, the coherence is at the D_7 level.

Comparing the D_8 and the D_7 correlation plots, it is clear that the latter reveal a coherent movement twice as fast as the former. Therefore, the passage from a coherence standing wave on D_8 to a coherent standing wave on D_7 means that the standing wave doubles its speed across the bifurcation. This phenomenon is somehow the reverse of the well-known period doubling phenomenon in chaos [20], and was recently formalized under the "period halving" bifurcation [7].

8. Conclusion

First, Case Study I, when combined with the recent results of [12], further reinforces the reproducibility of the early results of [1], indicating that the spinal wave is a coherent movement elicited by a central pattern generator. Here *reproducibility* spans across a broad population of subjects and across a period of more than 10 years, during which many changes in the protocol and the experimental hardware occurred, hence demonstrating the "robustness" of the results. Refs. [1,12], as well as Case Study I, have demonstrated coherence at the D_8 subband of the DB3 wavelet decomposition. Second, the really novel result here is the observation that the standing wave—revealing the neuro-physiologically relevant coherence at a distance [6]—can undergo a bifurcation with a shift of the coherence from D_8 to D_7. More practically speaking, this means that the motion speeds by a factor of 2, in a process that has recently been formalized under the terminology of "period halving" [7]. One interpretation of this finding could be a higher tension pattern in the spine elicited after the bifurcation. From a more conceptual point of view, a period-halving is a transition *away* from chaos. We have observed by working on quadriplegic patients that in general their sEMG signals are more chaotic than control subjects. Thus the bifurcation might be interpreted as the nervous system going to a less chaotic attractor.

The statistical test of the shift of the mean of the cross power spectral density corroborates the shift of the zero correlation nodes from the D_8 subband, before the bifurcation, to the D_7 subband, after the bifurcation. This statistical test confirms a structural change in the power spectrum of the signal as the system passes through a period-halving bifurcation; at low frequencies the power of the signal before the bifurcation turned out to be statistically significantly higher than the power of the signal after the bifurcation, and at high frequencies the power of the signals before and after the bifurcation is the reverse. The latter is to be interpreted with the restriction that this happens to be prevalent among the lower spine signals (lumbar spine and sacrum), when the sacral oscillator is better engaged than the cervical one.

It is hoped that the fundamental technique developed in this paper—the combination of coherence at D_8 versus D_7 together with inferential statistics on the shift of the mean of the cross PSDs—will be applicable to confirm other bifurcations, which as already argued are likely to happen in such complex neuro-skeletal systems.

Finally, while coherence at a distance is recognized to be the sign that the nervous system is able to orchestrate the motion

of many muscle masses to achieve a synergy [6], the more subtle features of whether coherence occurs at D_8 or D_7, or possibly at yet another subband, and how easily/how difficult it is for the neuro-physiological system to undergo the bifurcations remain to be assess in terms of their physiological relevance.

Acknowledgment

Dr. Kosko's help in developing the test of Section 5.2 is gratefully acknowledged.

References

[1] E. Jonckheere, P. Lohsoonthorn, S. Musuvathy, V. Mahajan, M. Stefanovic, On a standing wave central pattern generator and the coherence problem, Biomed. Signal Process. Control (2010) 336–347.
[2] N. Kopell, We got rhythm: dynamical systems of the nervous system, Notice Am. Math. Soc. 47 (1) (2000).
[3] A. Breig, Adverse Mechanical Tension in the Central Nervuous System, John Wiley, New York, 1987.
[4] A. Tilton, P.G. Mehta, Control with rhythms: a CPG architecture for pumping a swing, in: American Control Conference (ACC), Portland, OR, USA, 2014.
[5] E.A. Jonckheere, P. Lohsoonthonrn, Spatio-temporal analysis of an electrophysiological wave phenomenon, 2004, Leuven, Belgium.
[6] S.F. Farmer, Rhythmicity, synchronization and binding in human and primate motor systems, J. Physiol. 509 (1998) 3–14.
[7] R. Ndoundam, Period-halving bifurcation of a neuronal recurrence equation, Complex Syst. 20 (2012) 325–349.
[8] Y.A. Kuznetsov, Elements of Applied Bifurcation Theory. Applied Mathematical Sciences, vol. 112, Springer-Verlag New York, Inc, 1998.
[9] E.A. Jonckheere, P. Lohsoonthorn, R. Boone, Dynamic modeling of spinal electromyographic activity during various conditions, in: Proceeding of the American Control Conference, Denver, CO, 2003, pp. 465–470, Biomedical applications session.
[10] P. Lohsoonthorn, E.A. Jonckheere, Nonlinear switching dynamics in surface electromyography of the spine, in: Physics and Control, St. Petersbourg, Russia, 2003, pp. 277–282.
[11] S. Day, Important factors in surface EMG measurement, Tech. rep., Bortec Biomedical Ltd, Calgary, AB, Canada, 2000.
[12] R. Martin del Campo, E. Jonckheere, Stationary regime for standing wave central pattern generator, in: 3rd IEEE Global Conference on Signal and Information Processing (GlobalSIP 2015), Symposium on Signal Processing and Mathematical Modeling of Biological Processes with Applications to Cyber-Physical Systems for Precise Medicine, IEEE, Orlando, FL, 2015, pp. 913–917.
[13] K. Nakada, T. Asai, H. Hayashi, Burst Synchronization in Two Pulse-coupled Resonant-and-Fire Neuron Circuits, 218/2006, Springer, 2006, pp. 285–294.
[14] Y.M. Hawwar, A.M. Reza, R.D. Turney, Filtering (Denoising) in the Wavelet Transform Domain, CORE Solutions Group, Xilinx, Inc., 2004.
[15] Mallat, A theory for multiresolution signal decomposition: the wavelet representation, IEEE Pattern Anal. Mach. Intell. 11 (1989) 674–693.
[16] I. Daubechies, Ten Lectures on Wavelets, SIAM, 1992.
[17] M.G. Bulmer, Principles of Statistics, Dover, 1979.
[18] W. Mendenhall, T. Sincich, Statistics for Engineering and the Sciences, 5th ed., Prentice Hall, 2007.
[19] R. Martin del Campo, E. Jonckheere, Stationary versus bifurcation regime for standing wave central pattern generator, Tech. rep., University of Southern California, 2015.
[20] T. Tel, M. Gruiz, Chaotic Dynamics: An Introduction Based on Classical Mechanics, Cambridge University Press, Budapest, 2006.